Landslide Susceptibility Mapping Using Weight of Evidence (WoE) Method in Monterrey Metropolitan Area, Mexico

Luis Eduardo Arista-Cázares[1], Fabiola D. Yépez-Rincón[1*], Kevin David Rodríguez-González[1], Nelly Lucero Ramírez-Serrato[2], Héctor de León Gómez[1]

[1]Universidad Autónoma de Nuevo León, Civil Engineering Faculty, Department of Geomatics, San Nicolás de los Garza, Nuevo León, México
[2]Universidad Nacional Autónoma de México, Natural Resources Department, Mexico City, México

*fabiola.yepezrn@uanl.edu.mx

Keywords: Landslide susceptibility, landslide inventory, weight of evidence (WoE), ROC curve, Monterrey Metropolitan Area.

Abstract

The Monterrey Metropolitan Area (MMA), characterized by complex lithology, rugged topography, intense rainfall, and increasing anthropogenic pressures, faces increasing landslide hazards. This study applies a quantitative approach using the weight of evidence (WoE) method to assess landslide susceptibility across the MMA. A total of 292 historical landslide events were mapped using aerial imagery and archival data, with a 70/30 split for model training and validation. Twelve conditioning factors—including slope, lithology, elevation, hydrology, and land use—were analyzed to determine their influence on landslide occurrence. The resulting susceptibility map was classified into five risk categories using the Natural Breaks method. Model validation using the Receiver Operating Characteristic (ROC) curve yielded an Area Under the Curve (AUC) value of 0.77, indicating good predictive accuracy. These results demonstrate the effectiveness of the WoE method in landslide susceptibility mapping and provide a valuable tool for risk management and territorial planning in the region.

1. Introduction

Landslides are geodynamic phenomena that severely affect mountainous regions with urban occupation, generating both material and social impacts. Various factors, including uncontrolled urban expansion, land use changes, and an increase in the frequency of extreme weather events, have intensified the population's exposure to these processes (Alcántara-Ayala, 2025).

The Monterrey Metropolitan Area (MMA) in Mexico has been experiencing landslides due to its location in a valley surrounded by mountains. Rapid population growth has led to urban development on the hillsides, which increases vulnerability to these landslides. Additionally, extraordinary rainfall associated with hurricanes, such as Category 1 Hurricane Hanna in July 2020 and Tropical Storm Alberto in June 2024, contributes to the problem. As climate change is expected to increase the frequency of such weather events, the risk to the area may rise further (Touma et al., 2019).

Among the various methods used to assess susceptibility to mass movements, the statistical approach of weight of evidence (WoE) has established itself as a solid alternative when an inventory of landslides and environmental layers with adequate resolution is available. This method allows quantitative relationships to be established between the occurrence of landslides and terrain-related factors, making it particularly useful in contexts where a reproducible, spatially based approach is required (Sujatha and Sudharsan, 2024).

In this context, the present study aims to assess the susceptibility to landslides in the MMA using the WoE method, integrating topographic, geological, and land cover factors, to generate technical input that contributes to risk management in this metropolitan region.

Previous studies have successfully implemented the WoE method for landslide susceptibility mapping in various geological contexts, often comparing its performance with other statistical and machine learning techniques such as logistic regression (LR), support vector machine (SVM) and random forest (Hussain et al., 2021; Nwazelibe et al., 2023), where WoE has been shown to provide robust and interpretable results when a reliable landslide inventory is available, justifying its use as a reference approach in this research.

1.1 Study Area

The study area covers approximately 1409 km² in northeastern Nuevo León, Mexico (Figure 1). The MMA comprises thirteen municipalities with an estimated population of 5.3 million inhabitants, making it the second-largest metropolitan area in the country after Mexico City (Instituto Nacional de Estadística y Geografía, INEGI, 2020).

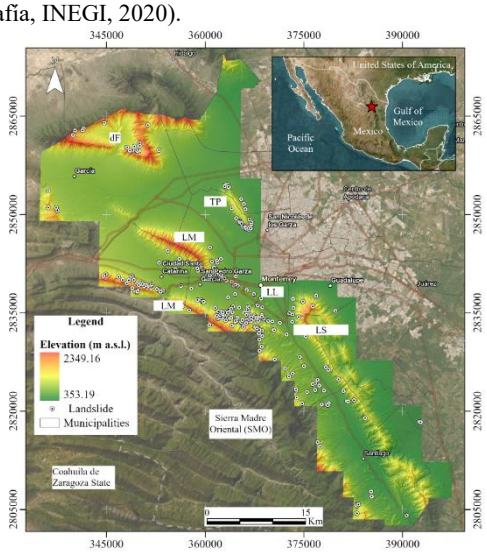

Figure 1. Location of the study area showing elevation and mapped landslide inventory. Abbreviations of anticlines: LS: La Silla, LM: Los Muertos, LL: Loma Larga, LM: Las Mitras, TP: Topo Chico, dF: del Fraile.

Morphologically, this area is located in a valley surrounded by mountains that form part of the Sierra Madre Oriental, which is characterized by a heterogeneity of sedimentary rocks, folded and thrust by tectonic effects (Padilla y Sánchez, 1982), favoring the generation of steep slopes and unstable areas, which the mountains have peaks over 2300 m .a.s.l. with valley floors of 350 m.

The region has a semi-arid climate (BSh according to the modified Köppen classification), in a transition between the sub-humid tropics and the desert (Aguilar Barajas and Ramírez Orozco, 2021), with an average annual temperature of around 23.6 °C (Comisión Nacional del Agua, CONAGUA, 2024a) and average annual precipitation of 650.2 mm (CONAGUA, 2024b), concentrated mainly in the summer months during the hurricane season.

In terms of its hydrography, the MMA is crossed by major watercourses, including the Santa Catarina River, which runs from east to west through the central portion of the MMA, the La Silla River to the south, and the Pesquería River to the north.

In brief, the physical and climatic conditions, rapid urban expansion, particularly on hillsides, have intensified pressure on the physical environment, altering the geomorphological balance and increasing vulnerability to landslides.

2. Methodology

A comprehensive overview of the methodology is presented in Figure 2.

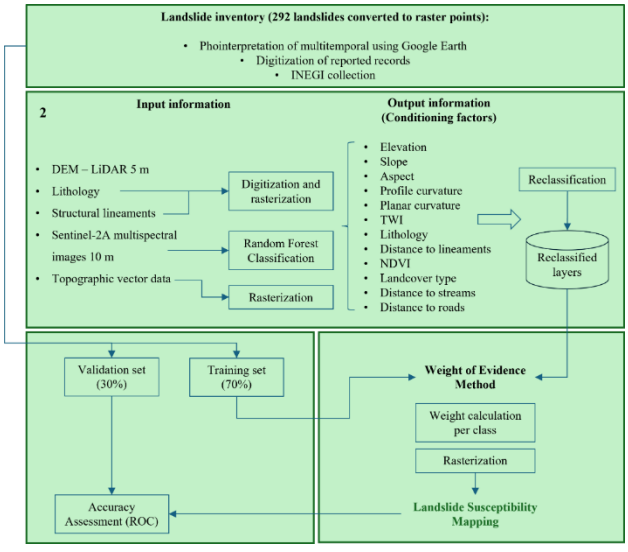

Figure 2. Methodological workflow for landslide susceptibility mapping in the study area.

2.1 Landslide Inventory Map

The use of a landslide inventory map is essential in this study, as the WoE method relies on the assumption that past events are indicative of future occurrences. Accordingly, this layer constitutes a fundamental input for landslide susceptibility assessment (Kontoes et al., 2021).

The inventory was compiled from multiple sources, including official records from INEGI (https://gaia.inegi.org.mx/mdm6/), municipal reports, news articles, time-series photointerpretation using Google Earth®, and field observations. A total of 292 landslides were identified within the study area and digitized as point features, which were subsequently converted into raster format using ArcGIS Pro environment (Figure 1).

Figure 3 illustrates different types of landslides in the MMA, including their causes and vulnerability to occurrence, which is primarily due to lithology, karst processes, precipitation, and irregular settlements.

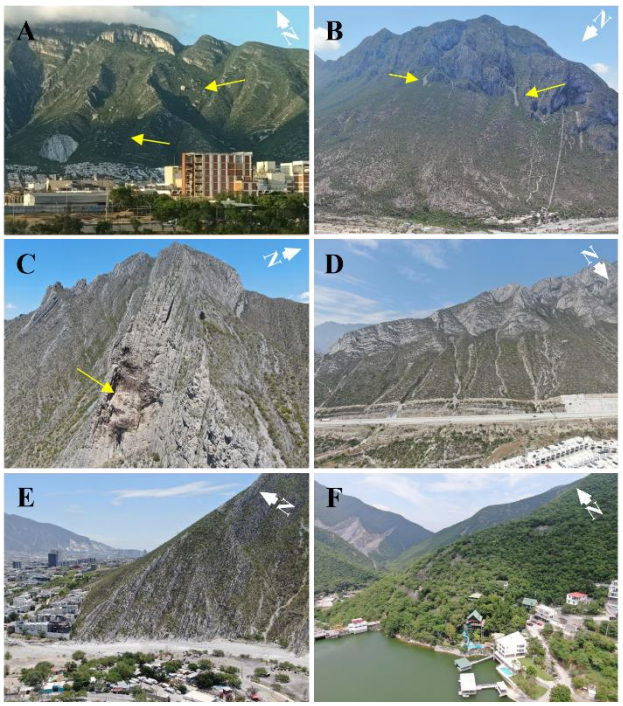

Figure 3. Examples of location and causes of landslides in the study area with aerial photographs. (A) Rock falls in the central portion of the southwestern flank of Las Mitras anticline; (B, C) Landslides near the “Grutas de García” and karstification processes as local causes of landslides in the del Fraile anticline; (D) Debris flow tracks on the southwest-facing slopes of the Los Muertos anticline; (E, F) Vulnerability to landslides due to irregular settlements in the Los Muertos anticline and in the central portion of the La Silla anticline.

The complete inventory was randomly divided into two subsets: 70% of the data were used to train the susceptibility model, while the remaining 30% were reserved for model validation.

2.2 Landslide Conditioning Factors

In this study, twelve conditioning factors were selected to develop the landslide susceptibility model (LSM), encompassing topographic, geological, hydrological, vegetation-related, and anthropogenic variables. The selection was based on previous studies conducted in similar contexts (Montalvo-Arrieta et al., 2010; Chapa-Guerrero et al., 2017; Ramírez-Serrato, 2019; Salinas-Jasso et al., 2020). These factors include elevation, slope, aspect, profile curvature, planar curvature, TWI (topographic wetness index), lithology, distance to lineaments, NDVI

(normalized difference vegetation index), landcover type, distance to streams, and distance to roads.

All input layers were prepared and processed in ArcGIS Pro, generating raster outputs with a spatial resolution of 5 m and projected using the WGS 84 UTM Zone 14 coordinate system. This spatial resolution was selected according to the highest freely available accuracy, corresponding to the LiDAR-derived terrain DEM provided by INEGI (https://www.inegi.org.mx/app/mapa/espacioydatos/).

Elevation has been widely used in landslide susceptibility analyses (e.g., Batar and Watanabe, 2021; Hussain et al., 2022) and was reclassified into five classes in this study, with values ranging from 323 to 2,349 m a.s.l. (Figure 4A).

Slope is one of the main factors in landslide occurrence, particularly in areas with complex mountainous morphology, such as the MMA. In this study, slope values ranged from < 15° to 87° and were reclassified into five classes with a 10° interval (Figure 4B).

Aspect represents the orientation of the slope concerning cardinal directions, which is exposed to environmental conditions that can influence the instability of rock masses (Qazi et al., 2023). It was reclassified into nine classes (Figure 4C).

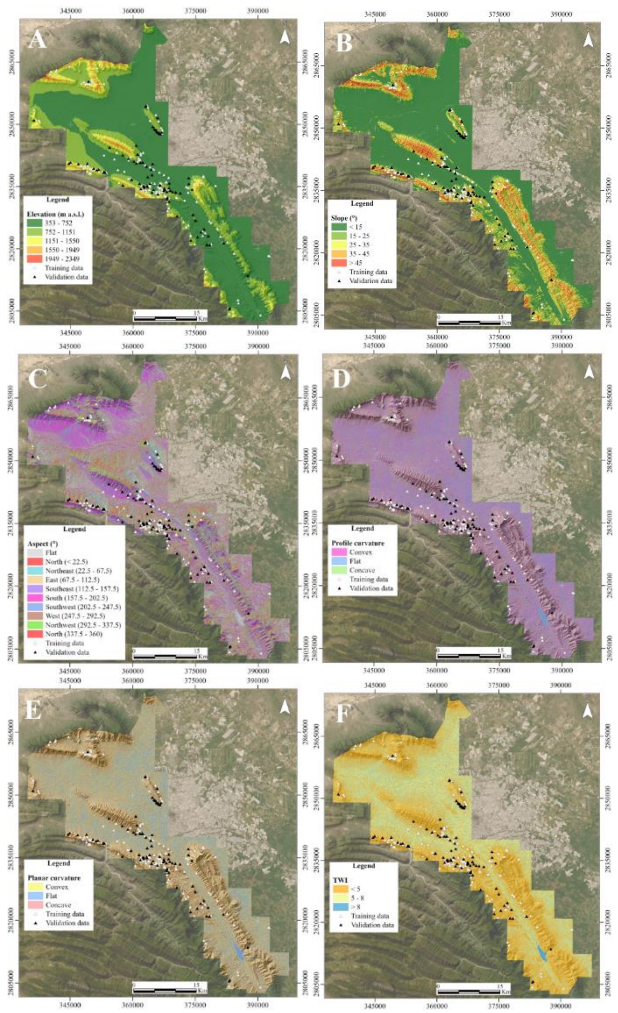

Figure 4. *Cont.*

Curvature describes the geometric shape of the terrain surface. Profile curvature is measured along the direction of the slope. Indicates the acceleration (concave) or deceleration (convex) of surface flow. Planar curvature, measured perpendicular to slope direction, reflects the convergence or divergence of the flow (Achu et al., 2023). Both curvature types were reclassified into three categories: concave, flat, and convex (Figures 4D and E, respectively).

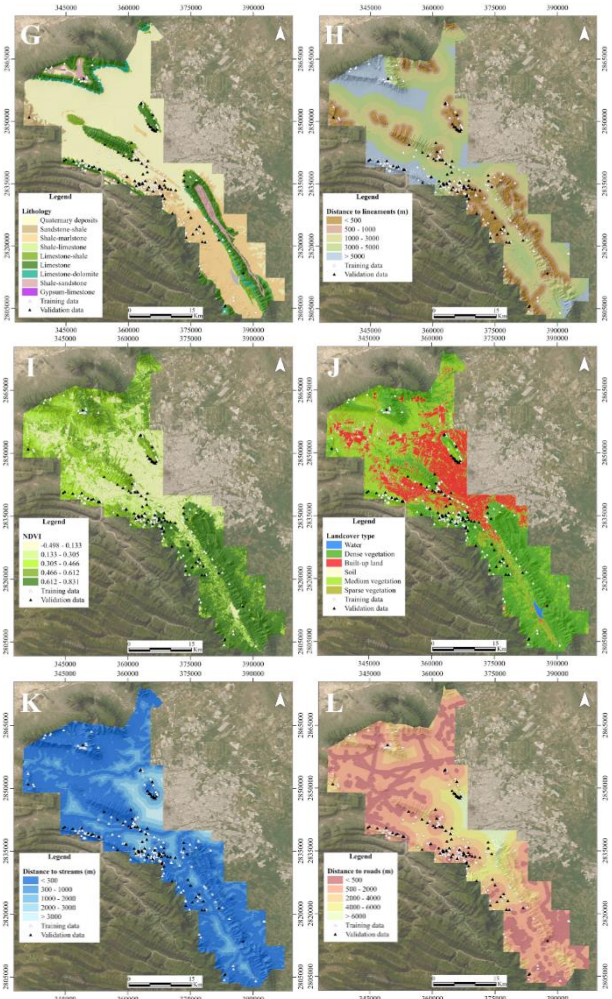

Figure 4. Landslide conditioning factors for the study area: (A) elevation; (B) slope; (C) aspect; (D) profile curvature; (E) planar curvature; (F) topographic wetness index; (G) lithology; (H) distance to lineaments; (I) normalized difference vegetation index; (J) landcover type; (K) distance to streams; and (L) distance to roads.

TWI represents the potential for water accumulation on the surface and is a proxy for soil saturation and hydrological processes that influence slope instability (Karakas et al., 2023). In this study, three types of TWI (Figure 4F) were obtained using the following equation, calculated in ArcGIS Pro:

$$TWI = In\left(\frac{a}{tan\beta}\right) \quad (1)$$

where a is the specific catchment area (m² per unit width orthogonal to the flow direction), and β is the slope gradient in radians.

Lithology is widely recognized as a key factor influencing landslide susceptibility (Dornik et al., 2022; Basharat et al., 2023). The study area is characterized by a diverse collection of folded and thrusted sedimentary rocks, formed through the tectonic deformation associated with the Sierra Madre Oriental orogenic belt. For this research, a lithological map was created by vectorizing and rasterizing geological maps with a scale of 1:50,000, provided by the Servicio Geológico Mexicano (SGM) and INEGI. The resulting raster layer was then reclassified into nine lithological units: Quaternary deposits, sandstone-shale, shale-marlstone, shale-limestone, limestone-shale, limestone, limestone-dolomite, shale-sandstone, and gypsum-limestone (see Figure 4G).

Recording structural lineaments, this factor considers the presence of fractures and faults that may act as zones of weakness within the relief's stratigraphy. To quantify this factor, the Euclidean Distance tool in ArcGIS Pro was applied to calculate the distance from each raster cell to the nearest mapped lineament. The resulting layer was reclassified into five distance classes (Figure 4H).

NDVI represents vegetation dynamics and surface conditions and has been widely used as a conditioning factor in landslide susceptibility assessments (e.g., Zhou et al., 2021). Vegetation influences slope stability by enhancing soil cohesion through root systems and reducing surface runoff. NDVI values range from -1 to +1, where positive values indicate the presence of vegetation, while negative values correspond to bare soil, urban areas, or water bodies. In this study, NDVI was calculated from a Sentinel-2A multispectral image in Google Earth Engine with a spatial resolution of 10 m, using the following equation:

$$NDVI = \frac{IR - R}{IR + R} \tag{2}$$

Where IR is the infrared and R is the red bands of the electromagnetic spectrum. In this study, NDVI varies from -0.5 to 0.83, and it was reclassified into five classes (Figure 4I).

Landcover type is influenced by both climate and human activities, which can contribute to the occurrence of landslides (Chen et al., 2019a; Pacheco-Quevedo et al., 2023). In this study, land cover type was determined using a Sentinel-2A multispectral image acquired on August 22, 2020, through Google Earth Engine. The classification process utilized the Random Forest machine learning algorithm, based on stratified random sampling and incorporating both NDVI and SAVI (soil adjusted vegetation index) indices. The SAVI index, in particular, has shown improved performance in differentiating vegetation (e.g., Illán-Fernández et al., 2024; Rodríguez González et al., 2024). A total of 378 sample points were selected, with 80% allocated for training and 20% for validation. The final classification categorized land cover into six classes: water, soil, built-up areas, dense vegetation, medium vegetation, and sparse vegetation (see Figure 4J). The model achieved an overall accuracy of 89.65% and a Kappa coefficient of 0.87, as indicated by the confusion matrix. The resulting classification map was then exported and integrated into ArcGIS Pro, where it was resampled from 10 to 5 m using the nearest neighbour method to ensure spatial compatibility with the other conditioning factors derived from the 5-m LiDAR-based terrain DEM.

Distances to streams and roads were calculated from the drainage and road networks provided in the topographic vector dataset from INEGI. These vector layers were converted to raster format, and Euclidean distances were calculated in ArcGIS. Both resulting rasters were subsequently reclassified into five distance classes to standardize the information (Figures 4K and 4L).

2.3 WoE method

In this study, the WoE method was applied to generate the landslide susceptibility model. This approach is based on the principles of Bayesian probability, as proposed by Bonham-Carter et al. (1989). It enables the combination of multiple evidence layers to estimate the probability of a specific event occurring. Its core principle lies in evaluating the spatial association between each conditioning factor and the presence or absence of landslide events (Zhang et al., 2023).

The method assigns a statistical weight to each class within a conditioning factor reflecting its relative influence on landslide occurrence. These weights are calculated based on the presence (W^+) and absence (W^-) of landslide events within each class, as defined by:

$$W^+ = log_e \frac{P\{B|D\}}{P\{B|\underline{D}\}} \tag{3}$$

$$W^- = log_e \frac{P\{\underline{B}|D\}}{P\{\underline{B}|\underline{D}\}} \tag{4}$$

where P is the probability, B is the presence of a desired class of landslide conditioning factor, $\underline{B}$ is the absence of a desired class of landslide conditioning factor, D is the presence of landslides, and $\underline{D}$ is the absence of landslides. Each class of conditioning factor was calculated using Eqs. 3 and 4. The difference between the positive and negative weights is referred to as the weight contrast (C), calculated as $C = W^+ - W^-$. The magnitude of this contract reflects the overall spatial association between each class of a conditioning factor and the occurrence of landslides. A positive C value ($C > 0$) indicates a positive correlation, meaning that landslides are more likely to occur in that class. In contrast, a negative C value ($C < 0$) suggests a negative correlation, where landslides are less likely to occur.

The Landslide Susceptibility Index (LSI) map was produced by summing the weights of all conditioning factors using the Map Algebra tool in ArcGIS Pro, following the equation:

$$LSM_{Wf} = (W_{f\ Elevation}) + (W_{f\ Slope}) + (W_{f\ Aspect}) + (W_{f\ Profile\ curvature}) + (W_{f\ Planar\ curvature}) + (W_{f\ TWI}) + (W_{f\ Lithology}) + (W_{D.to\ lineaments}) + (W_{f\ NDVI}) + (W_{f\ Landcover\ type}) + (W_{f\ D.to\ streams}) + (W_{f\ D.to\ roads}) \tag{5}$$

2.4 Validation method

The performance of the landslide susceptibility map was assessed using the Relative Operating Characteristic (ROC) method and by calculating the percentage of observed landslides falling within each susceptibility class. The area under the ROC curve (AUC) reflects the quality of the probabilistic model and its capacity to discriminate between the occurrence and non-occurrence of landslides. An AUC value approaching 1 denotes high predictive accuracy, whereas a value near 0.5 indicates poor performance (Bui et al., 2014). In this study, the success-rate curves were generated using Python 3.12.

3. Results and Discussion

3.1 Landslide Susceptibility Model

The WoE values for all conditioning factors are presented in Table 1. The resulting landslide susceptibility index ranges from –14.29 to 10.76 and was reclassified using the Jenks natural breaks method (Jenks and Caspall, 1971) into five susceptibility classes: Very Low, Low, Moderate, High, and Very High (Figure 5). This method is among the most widely applied in landslide susceptibility modeling (Qazi et al., 2023), as it is particularly suitable for datasets that are not normally distributed. It minimizes within-class variance and maximizes between class differences, providing a data-driven categorization that better reflects the intrinsic distribution of susceptibility values (Chen et al., 2019b; Abdo et al., 2024).

The analysis of evidence weights determines that slope is the factor with the greatest influence on the occurrence of landslides, with particularly high contrast values in the classes 35–45° (C = 1.860), > 45° (C = 1.534), and 25–35° (C = 1.380). These results coincide with those reported by Aslam et al. (2022) and Al-kordi et al. (2025), who point out that landslides tend to concentrate in intermediate to high slope intervals, where the gravitational potential energy is sufficient to overcome the shear strength of the materials.

In terms of lithology, limestone–shale (C = 1.757) and limestone (C = 1.513) units show the strongest positive association with the occurrence of landslides. This behavior can be attributed to the presence of inclined stratification planes, intercalations of materials with different resistances, and dissolution processes in limestone, which generate areas of weakness. Moreover, the alternation of limestone and shale also favors water infiltration and accumulation, reducing the cohesion of the material (Do et al., 2022).

Distance to lineaments (< 500 m; C = 1.085) shows the influence of fractures and faults as areas of preferential weakness for the development of mass movements, a pattern documented in various geological contexts.

The altitudinal analysis indicates that the interval of 752–1151 m (C = 1.546) is the most susceptible, which could be explained by its coincidence with mid-slope and foothill areas, where steep slopes, the presence of roads, and greater human occupation converge, factors that increase pressure on the stability of the terrain.

In terms of aspect, the south class (C = 0.382) affects the activation of landslides. Regarding profile curvature and planar curvature, the highest values are convex (C = 0.773) and concave (C = 0.420), respectively.

TWI values < 5 (C = 1.061) suggest that landslides are concentrated in areas with lower surface flow accumulation, possibly related to convex slopes or interfluves, where infiltration is more effective and may favor increased pore pressures at depth.

Concerning landcover type, areas of dense vegetation (C = 0.413) and medium vegetation (C = 0.257) show moderate positive associations. Although vegetation usually stabilizes the terrain, in this case, it could reflect the spatial distribution of landslides in areas of slopes covered by dense forest or scrub, where the topography and lithology already predispose them to instability, and where intense precipitation events can overcome the stabilizing effect of the roots (Pacheco-Quevedo et al., 2023).

Finally, the Distances to streams (300–1000 m; C = 0.558) and roads (500–2000 m; C = 0.585) reinforce the hydrological factors and influence of anthropogenic factors as risk modulators. Streams contribute to basal undermining and lateral erosion, reducing the stability of adjacent slopes, while the roads can generate slope cuts and runoff concentrations.

Parameter	Class	Area (km^2)	Landslides	W+	W-	C
Elevation (m)	353 - 752	939.85	71	-0.724	0.838	-1.563
	752 - 1151	346.65	109	1.001	-0.546	1.546
	1151 - 1550	98.03	22	0.540	-0.049	0.589
	1550 - 1949	28.04	2	-0.786	0.012	-0.798
	1949 - 2349	0.68	0	NA	NA	NA
Slope (°)	< 15	905.91	38	-1.348	1.057	-2.405
	15 - 25	140.32	21	0.043	-0.005	0.048
	25 - 35	161.16	56	1.150	-0.230	1.380
	35 - 45	141.66	63	1.558	-0.302	1.860
	> 45	62.96	26	1.429	-0.105	1.534
Aspect	Flat	3.57	0	NA	NA	NA
	North (< 22.5)	111.93	20	0.255	-0.024	0.279
	Northeast (22.5 - 67.5)	260.40	39	0.044	-0.010	0.054
	East (67.5 - 112.5)	228.38	25	-0.316	0.053	-0.369
	Southeast (112.5 - 157.5)	179.03	24	-0.085	0.012	-0.097
	South (157.5 - 202.5)	179.34	34	0.328	-0.054	0.382
	Southwest (202.5 - 247.5)	143.68	25	0.223	-0.028	0.250
	West (247.5 - 292.5)	106.11	17	0.124	-0.011	0.134
	Northwest (292.5 - 337.5)	113.68	9	-0.673	0.045	-0.719
	North (337.5 - 360)	85.88	11	-0.138	0.008	-0.146
Profile curvature	Concave	771.76	91	-0.232	0.236	-0.468
	Flat	202.66	18	-0.548	0.073	-0.621
	Convex	442.08	95	0.485	-0.289	0.773
Planar curvature	Concave	656.61	113	0.209	-0.211	0.420
	Flat	315.33	15	-1.217	0.209	-1.425
	Convex	444.56	76	0.201	-0.103	0.304
TWI	< 5	701.08	145	0.436	-0.625	1.061
	5 - 8	590.56	51	-0.579	0.303	-0.881
	> 8	123.62	8	-0.891	0.060	-0.951
Lithology	Quaternary deposits	689.21	19	-1.783	0.709	-2.492
	Sandstone - shale	19.54	3	0.073	-0.001	0.074
	Limestone	320.31	102	1.019	-0.494	1.513
	Limestone - dolomite	9.62	0	NA	NA	NA
	Limestone - shale	76.77	35	1.603	-0.153	1.757
	Shale - sandstone	206.89	34	0.154	-0.028	0.182
	Shale - limestone	34.82	4	-0.262	0.006	-0.268
	Shale - marlstone	51.11	7	-0.061	0.002	-0.063
	Gypsum - limestone	0.49	0	NA	NA	NA
Distance to lineaments (m)	< 500	189.18	55	0.888	-0.197	1.085
	500 - 1000	155.42	26	0.175	-0.023	0.199
	1000 - 3000	494.38	51	-0.382	0.169	-0.551
	3000 - 5000	343.52	26	-0.722	0.168	-0.890
	> 5000	230.65	46	0.390	-0.090	0.480
NDVI	-0.5 - 0.13	242.15	16	-0.868	0.125	-0.994
	0.13 - 0.30	167.35	21	-0.161	0.020	-0.182
	0.30 - 0.47	240.17	51	0.469	-0.118	0.587
	0.47 - 0.61	322.80	58	0.262	-0.088	0.349
	0.61 - 0.83	440.70	58	-0.107	0.046	-0.152
Landcover type	Water	5.55	0	NA	NA	NA
	Dense vegetation	583.83	102	0.228	-0.185	0.413
	Built-up level	271.80	18	-0.866	0.143	-1.009
	Soil	23.69	0	NA	NA	NA
	Medium vegetation	373.76	63	0.184	-0.073	0.257
	Sparse vegetation	155.13	21	-0.074	0.009	-0.083
Distance to streams (m)	< 300	916.08	120	-0.112	0.185	-0.297
	300 - 1000	314.91	64	0.414	-0.144	0.558
	1000 - 2000	130.07	20	0.075	-0.008	0.083
	2000 - 3000	40.91	0	NA	NA	NA
	> 3000	12.78	0	NA	NA	NA
Distance to roads (m)	< 500	362.99	27	-0.741	0.183	-0.924
	500 - 2000	607.91	113	0.303	-0.281	0.585
	2000 - 4000	301.84	41	-0.070	0.018	-0.089
	4000 - 6000	106.22	16	0.051	-0.004	0.055
	> 6000	34.21	7	0.423	-0.012	0.435

Table 1. Calculated the weight for classes of conditioning factors per class based on landslide occurrences.

In this study, the results of the WoE model were used as inputs to assess multicollinearity among the conditioning factors using the variance inflation factor (VIF), which measures the degree to

which a variable correlates linearly with other factors. A VIF value greater than 10 is commonly considered indicative of strong correlation (Bui et al., 2011). The analysis revealed that NDVI, elevation, and dense vegetation had VIF values above 10, indicating strong correlation with other factors. Despite this, these conditioning factors were retained in the analysis to preserve critical information on landslide occurrences, including the 102 events recorded in the dense vegetation category.

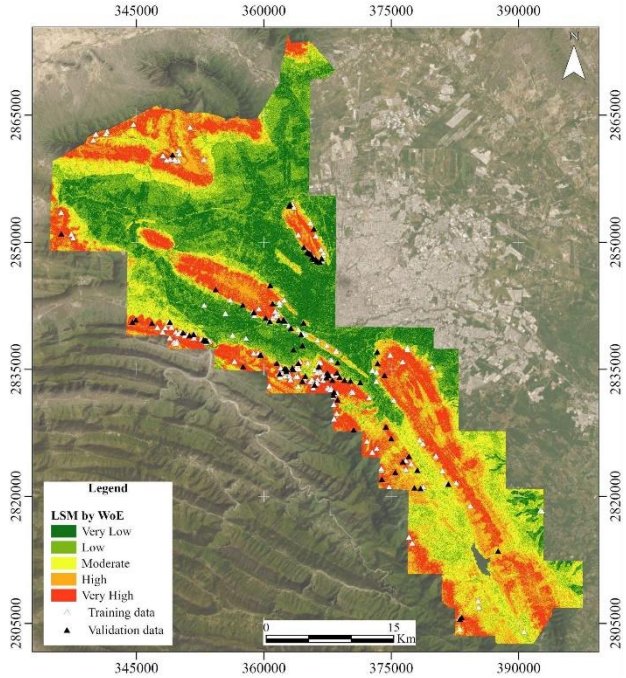

Figure 5. Landslide susceptibility model using the weight of evidence method with distribution per class.

The relative importance of conditioning factors was calculated based on the absolute WoE values for each category. As shown in Figure 6, slope, lithology, and elevation contributed the most to landslide occurrence, with relative contributions of 19.2%, 16.9%, and 11.9%, respectively. TWI also played a notable role, contributing 7.7%, while the remaining factors had a lower influence.

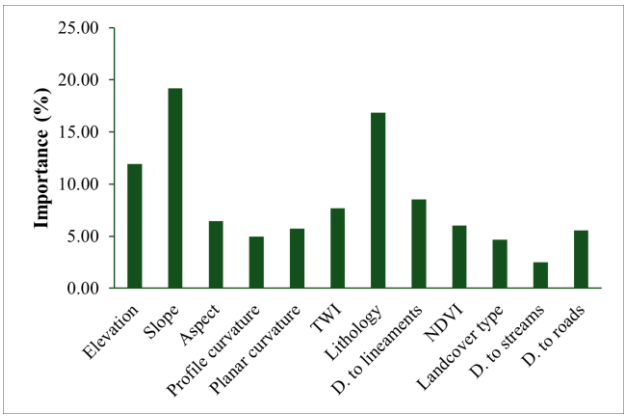

Figure 6. Conditioning factors importance of landslide.

The area and percentage of each class are shown in Table 2, along with the number of landslides. 8.56% of the mapped landslides were located in areas classified as very low or low susceptibility. This mismatch suggests potential limitations of the WoE model in fully capturing the spatial complexity of landslide occurrence. The discrepancy may arise from factors not included in the conditioning dataset, the resolution of the input layers, or the assumption of conditioning independence inherent to the method. While such misclassifications are common in susceptibility modeling, they highlight the need for incorporating additional variables or more advanced methods to improve predictive accuracy.

Susceptibility	Area (km^2)	Percentage (%)	Number of landslide
Very low	296.31	21.02	7
Low	329.17	23.35	18
Moderate	269.61	19.13	32
High	257.77	18.29	64
Very high	256.67	18.21	171

Table 2. Percentage of area occupied by susceptibility zones.

3.2 Validation of Landslide Susceptibility Map

The validation results indicate that the WoE model achieved an AUC value of 0.77 in the success-rate curve (Figure 7), which suggests an acceptable predictive capacity (range of 0.7-0.8) for identifying areas prone to landslides according to Abul Hasanat et al. (2010). This means that the present model can distinguish, with reasonable accuracy, between stable and unstable slopes.

This performance is consistent with previous studies that applied the WoE method in mountainous environments with similar conditioning factors (e.g., Liu and Duan, 2018; Alsabhan et al., 2022). Moreover, the obtained AUC value (0.77) falls within the range typically reported for other statistical and machine learning approaches such as LR, SVM, or RF models, indicating that the WoE approach achieves comparable predictive accuracy while maintaining transparency in the weighting of conditioning factors (Polykretis and Chalkias, 2018; Naceur et al., 2022). Specifically for MMA, this represents the first validation of a WoE-based susceptibility model; therefore, this result provides a baseline for future studies in the region.

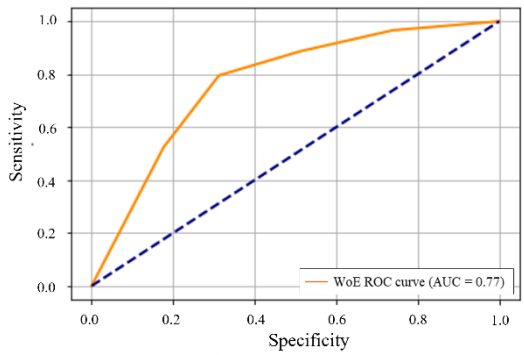

Figure 7. Validation of landslide susceptibility model under the ROC (AUC) by the weight of evidence method.

4. Conclusion

In this study, we assess landslide susceptibility in the Monterrey Metropolitan Area. This study can help in defining the strategies that can best reduce casualties and property losses. Four statements can be concluded as follows:

This contribution has been peer-reviewed. The double-blind peer-review was conducted on the basis of the full paper.
https://doi.org/10.5194/isprs-annals-X-3-W3-2025-19-2026 | © Author(s) 2026. CC BY 4.0 License.

(1) Slope, lithology, and elevation are the dominant factors influencing landslide susceptibility in the Monterrey Metropolitan Area. Slopes between 25° and > 45°, limestone-shale and limestone lithologies, and elevations between 752–1151 m were strongly associated with landslide occurrences due to their inherent geological and topographic instability.

(2) Hydrological and structural variables also significantly modulate landslide risk. Low TWI values, proximity to faults (< 500 m), and intermediate distances to rivers (300–1000 m) indicate that both water infiltration dynamics and structural weaknesses contribute to slope failures.

(3) Anthropogenic factors such as proximity to roads and landcover patterns play a notable role in triggering landslides. Roads (500–2000 m from landslides) and areas with dense or medium vegetation saw moderate susceptibility, likely due to terrain modification and precipitation-driven events in forested, sloped regions.

(4) The landslide susceptibility model demonstrated good predictive performance, with an AUC value of 0.77, validating the effectiveness of the WoE method for mapping landslide-prone areas and supporting land-use planning and risk mitigation strategies, as well as representing the first validated susceptibility model in the MMA. However, the AUC value also reflects that there is still room for improvement, potentially by incorporating higher-resolution conditioning factors, more detailed landslide inventories, or integrating complementary statistical or machine learning approaches.

The methodological framework and findings of this study may be transferable to other mountainous and semi-arid regions affected by rainfall-induced landslides, for regional susceptibility assessment and land-use planning in similar geomorphological settings.

Acknowledgements

The authors thank the Secretariat of Science, Humanities, Technology, and Innovation (Secihti) for awarding scholarships to Luis Arista (CVU: 1347829) and Kevin David Rodríguez (CVU: 1014573) through the Graduate Program of the Faculty of Civil Engineering—Master of Science in Environmental Engineering and Doctorate in Engineering with a focus on Environmental Engineering—at the Autonomous University of Nuevo León. We also acknowledge the Department of Geomatics at the Institute of Civil Engineering for providing the tools and resources necessary to carry out this research.

References

Abul Hasanat, M.H., Ramachandram, D., Mandava, R., 2010. Bayesian belief network learning algorithms for modeling contextual relationships in natural imagery: a comparative study. *Artil Intell Rev*, 34, 291-308. https://doi.org/10.1007/s10462-010-9176-8

Achu, A.L., Aju, C.D., Di Napoli, M., Prakash, P., Gopinath, G., Shaji, E., Chandra, V., 2023. Machine-learning based landslide susceptibility modelling with emphasis on uncertainty analysis. *Geoscience Frontiers*, 14, 101657. https://doi.org/10.1016/j.gsf.2023.101657

Aguilar Barajas, I., Ramírez Orozco, A.I., 2021: *Agua para Monterrey Logros, retos y oportunidades para Nuevo León y México*. Segunda Edición. Instituto Tecnológico y de Estudios Superiores de Monterrey. https://hdl.handle.net/11285/642843

Al-kordi, H., Al-Amri, A., raju, G., 2025. Landslide susceptibility mapping using geospatial, analytical hierarchy process (AHP), and binary logistic regression (BLR) techniques – A study of Wadi Habban Basin, Shabwah, Yemen. *Results in Earth Sciences*, 3, 100103. https://doi.org/10.1016/j.rines.2025.100103

Alcántara-Ayala, I., 2025. Landslides in a changing world. *Landslides*. https://doi.org/10.1007/s10346-024-02451-1

Alsabhan, A., Singh, K., Sharma, A., Alam, S., Pandey, D.D., Rahman, S.A.S., Khursheed, A., Munshi, F.M., 2022. Landslide susceptibility assessment in the Himalayan range based along Kasauli – Parwanoo road corridor using weight of evidence, information value, and frequency ratio. *Journal of King Saud University - Science*, 34, 101759. https://doi.org/10.1016/j.jksus.2021.101759

Aslam, B., Maqsoom, A., Khalil, U., Ghorbanzadeh, O., Blaschke, T., Farooq, D., Tufail, R.F., Suhail, S.A., Ghamisi, P., 2022. Evaluation of Different Landslide Susceptibility Models for a Local Scale in the Chitral District, Northern Pakistan. *Sensors*, 22, 3107. https://doi.org/10.3390/s22093107

Basharat, M. ul., Khan, J.A., Abdo, H.G., Almohamad, H., 2023. An integrated approach based landslide susceptibility mapping: case of Muzaffarabad region, Pakistan. *Geomatics, Natural and Risk*, 14(1). https://doi.org/10.1080/19475705.2023.2210255

Batar, A.K., Watanabe, T., 2021. Landslide Susceptibility Mapping and Assessment Using Geospatial Platforms and Weights of Evidence (WoE) Method in Indian Himalayan Region: Recent Developments, Gaps, and Future Directions. *ISPRS Int. J. Geo-Inf.*, 10, 114. https://doi.org/10.3390/ijgi10030114

Bonham-Carter, G.F., 1989. Weights of evidence modelling: a new approach to mapping mineral potential. *Stat. Appl. Earth. Sci.* 89, 171-183.

Bui, D.T., Lofman, O., Revhaug, I. Dick, O., 2011. Landslide susceptibility analysis in the Hoa Binh province of Vietnam using statistcal index and logistic regression. *Nat Hazards*, 59, 1413-1444. https://doi.org/10.1007/s11069-011-9844-2

Bui, D.T., Pradhan, B., Revhaug, I., Trung Tran, C., 2014. A Comparative Assessment Between the Application of Fuzzy Unordered Rules Induction Algorithm and J48 Decision Tree Models in Spatial Prediction of Shallow Landslides at Lang Son City, Vietnam. In: Srivastava, P., Mukherjee, S., Gupta, M., Islam, T. (eds) Remote Sensing Applications in Environmental Research. Society of Earth Scientists Series. Springer, Cham. https://doi.org/10.1007/978-3-319-05906-8_6

Chapa-Guerrero, J.R., Méndez-Delgado, S., Chávez-Cabello,. G., Chapa-Arce, I., Ibarra-Martínez, S.E., 2017. Movimientos en masa, un riesgo geológico latente en el área metropolitana de Monterrey, N.L., México. Ciencia UANL, 19(82), 41-45.

Chen, L., Guo, Z., Yin, K., Shrestha, D.P., Jin, S., 2019a. The influence of land use and land cover change on landslide susceptibility: a case study in Zhushan Town, Xuan'en County (Hubei, China). *Nat. Hazards Earth Syst. Sci*., 19, 2207-2228. https://doi.org/10.5194/nhess-19-2207-2019

Chen, W., Sun, Z., Han, J., 2019b. Landslide Susceptibility Modeling Using Integrated Ensemble Weights of Evidence with Logistic Regression and Random Forest Models. *Appl. Sci*, 9, 171. http://dx.doi.org/10.3390/app9010171

CONAGUA, 2024a: Temperatura media por entidad federativa y nacional. Comisión Nacional del Agua (CONAGUA) https://smn.conagua.gob.mx/es/climatologia/temperaturas-y-lluvias/resumenes-mensuales-de-temperaturas-y-lluvias

CONAGUA, 2024b: Precipitación (mm) por entidad federativa y nacional. Comisión Nacional del Agua (CONAGUA) https://smn.conagua.gob.mx/es/climatologia/temperaturas-y-lluvias/resumenes-mensuales-de-temperaturas-y-lluvias

Do, N.H., Goto, S., Abe, S., Nguyen, K.T., Miyagi, T., Hayashi, K., Watanabe, O., 2022. Torrent rainfall-induced large-scale karst limestone slope collapse at Khanh waterfall, Hoa Binh Province, Vietnam. *Geoenvironmental Disasters*, 9(4). https://doi.org/10.1186/s40677-022-00206-5

Dornik, A., Drăguț, L., Oguchi, T., Hayakawa, Y., Micu, M., 2022. Influence of sampling design on landslide susceptibility modeling in lithologically heterogenous areas. *Sci Rep*, 12, 2106. https://doi.org/10.1038/s41598-022-06257-w

Hussain, M.L., Shafique, M., Bacha, A.S., Chen, X-q-. Chen, H-y., 2021. Landslide inventory and susceptibility assessment using multiple statistical approaches along the Karakoram highway, northern Pakistan. *J. Mt. Sci.,* 18, 583-598. https://doi.org/10.1007/s11629-020-6145-9

Hussain, M.A., Chen, Z., Kalsoom, I., Asghar, A., Shoaib, M., 2022. Landslide Susceptibility Mapping Using Machine Learning Algorithm: A Case Study Along Karakoram Highway (KKH), Pakistan. *J Indian Soc Remote Sens*, 50, 849-866. https://doi.org/10.1007/s12524-021-01451-1

Illán-Fernández, E., Tiede, D., Sudmanns, M., 2023. Consistent land use and land cover classification across 20 years of various high-resolution images for detecting soil sealing in Murcia, Spain. *Remote Sensing Applications: Society and Environment*, 35, 101223. https://doi.org/10.1016/j.rsase.2024.101223

INEGI, 2020: Censo nacional de población y vivienda. Instituto Nacional de Estadística y Geografía.

Jenks, G.F., Gaspall, F.C., 1971. Error on choroplethic maps: Definition, measurement, reduction. *Ann Assoc Am Geogr*, 61(2), 217-244.

Karakas, G., Kocaman, S., Gokceoglu., 2023. A Hybrid Multi-Hazard Susceptibility Assessment Model for a Basin in Elazig Province, Türkiye. *Int J Disaster Risk Sci*, 14, 326-341. https://doi.org/10.1007/s13753-023-00477-y

Kontoes, C., Loupasakis, C., Papoutsis, I., Alatza, S., Poyiadji, E., Ganas, A., Psychogyiou, C., Kaskara, M., Antoniadi, S., Spanou, N., 2021. Landslide Susceptibility Mapping of Central and Western Greece, Combining NGI and WoE Methods, with Remote Sensing and Ground Truth Data. *Land*, 10, 402. https://doi.org/10.3390/land10040402

Liu, J., Duan, Z., 2018. Quantative Assessment of Landslide Susceptibility Comparing Statistical Index, Index of Entropy and Weights of Evidence in the Shangnan Area, China. *Entropy*, 20(11), 868. https://doi.org/10.3390/e20110868

Montalvo Arrieta, J.C., Chávez-Cabello, G., Velasco-Tapia, F., 2010. Causes and effects of landslides in the Monterrey Metropolitan Area, NE Mexico. In: Werner, D., Friedman, H. (eds) Landslides: causes, types and effects. Nova Science Publishers, pp. 72-104.

Naceur, H.A., Abdo, H.G., Igmoullan, B., Namous, M., Almohamad, H., Al Dughairi, A.A., Al-Mutiry, M., 2022. Performance assessment of the landslide susceptibility modelling using the support vector machine, radial basis function network, and weight of evidence models in the N'fis river basin, Morocco. *Geoscience Letters*, 9(39). https://doi.org/10.1186/s40562-022-00249-4

Nwazelibe, V.E., Unigwe, C.O., Egbueri, J.C., Integration and comparison of algorithmic weight of evidence and logistic regression in landslide susceptibility mapping of the Orumba North erosion-prone region, Nigeria. *Model. Earth Syst. Environ*, 9, 967-986. https://doi.org/10.1007/s40808-022-01549-6

Pacheco-Quevedo, R., Velastegui-Montoya, A., Montalván-Burbano, N., Morante-Carballo, F., Korup, O., Rennó, C.D., 2023. Land use and land cover as a conditioning factor in landslide susceptibility: a literature review. *Landslides*, 20, 967-982. https://doi.org/10.1007/s10346-022-02020-4

Padilla y Sánchez, R.J., 1982: Geologic evolution of the Sierra Madre Oriental between Linares, Concepción del Oro, Saltillo and Monterrey, México. Ph.D. thesis, University of Texas.

Polykretis, C., Chalkias, C., 2018. Comparison and evaluation of landslide susceptibility maps obtained from weight of evidence, logistic regression, and artificial neural network models. *Nat Hazards*, 93, 249-274. https://doi.org/10.1007/s11069-018-3299-7

Ramírez-Serrato, N.L., 2019. Validación y diseño de predicción espacial para cartografiar susceptibilidad por deslizamientos en la Zona Metropolitana de Monterrey, N.L., México. Doctoral thesis, Universidad Autónoma de Nuevo León.

Rodríguez González, K.D., Arista Cázares, L.E., Yépez Rincón, F.D., 2024. Spatiotemporal land use land cover change analysis of urban narrow river using Google Earth Engine and Machine learning algorithms in Monterrey, Mexico. *ISPRS Ann. Photogramm. Remote Sens. Spatial Inf. Sci.,* X-3-2024, 371-375. https://doi.org/10.5194/isprs-annals-X-3-2024-371-2024, 2024

Salinas-Jasso, J.A., Velasco-Tapia, F., Montalvo-Arrieta, J.C., 2020. Landslide susceptibility assessment for the Monterrey Metropolitan Area, northeastern Mexico. In: Krogh, D.S. (ed) Landslides: monitoring, susceptibility and management. Nova Science Publishers.

Sujatha, E.R., Sudharsan, J.S., 2024. Landslide Susceptibility Mapping Methods - A Review. In: Panda, G.K., Shaw, R., Pal, S.C., Chatterjee, U., Saha, A. (eds) Landslide: Susceptibility, Risk Assessment and Sustainability. Advances in Natural and

Technological Hazards Research, vol 52. Springeer, Cham. https://doi.org/10.1007/978-3-031-56591-5_4

Touma, D., Stevenson, S., Camargo, S.J., Horton, D.E., Diffenbaugh, N.S., 2019. Variationss in the Intensity and Spatial Extent of Tropical Cyclone Precipitation. *Geophysical Research Letters*, 46(13), 992-14002. https://doi.org/10.1029/2019GL083452

Qazi, A., Singh, K., Vishwakarma, D.K., Abdo, H.G., 2023. GIS based landslide susceptibility zonation mapping using frequency ratio, information value and weight of evidence: a casenstudy in Kinnaur District HP India. Bull Eng Geol Environ, 82, 332. https://doi.org/10.1007/s10064-023-03344-8

Zhang, G., Wang, S., Chen, Z., Liu, Y., Xu, Z., Zhao, R., 2023. Landslide susceptibility evaluation integrating weight of evidence model and InSAR results, west of Hubei Province, China. *J. Remote Sens. Space Sci*. 26, 95–106. https://doi.org/10.1016/j.ejrs.2022.12.010

Zhou, X., Wu, W., Fu, X., 2021. Geoinformation-based landslide susceptibility mapping in subtropical area. *Sci Rep*, 11, 24325. https://doi.org/10.1038/s41598-021-03743-5